

Neural Networks Evaluating NMR Data: An Approach To Visualize Similarities and Relationships of Sol–Gel Derived Inorganic–Organic and Organometallic Hybrid Polymers¹

Frank Hoehn, Ekkehard Lindner,* and Hermann A. Mayer*

Institut für Anorganische Chemie der Universität Tübingen, Auf der Morgenstelle 18, D-72076 Tübingen

Thomas Hermle and Wolfgang Rosenstiel*

Wilhelm-Schickard-Institut für Informatik, Lehrstuhl für Technische Informatik der Universität Tübingen, Sand 13, D-72076 Tübingen

Received May 10, 2001

An artificial neural network (ANN)—the Kohonen Self-Organizing Feature Map (SOM)—is used to evaluate solid-state NMR spectroscopic derived data of 72 siloxane-based phosphine and organometallic functionalized hybrid polymers. The data set consists of parameters that describe their structural features and their dynamic behavior. The ANN visualizes similarities of the investigated compounds by reducing the dimension of the data set. This allows a comparison of these polymers that was not possible beforehand because of their structural diversity.

INTRODUCTION

One of the most important advantages of homogeneous catalysis is the possibility to control conversions and selectivities toward the desired products. The ambition to transfer these properties to supported catalysts in order to facilitate the separation of the reaction products from the catalyst has not been achieved in a satisfactory way. The severe problems of leaching of the catalyst from the polymer backbone has not been solved yet.² In addition, the knowledge about the nature of reactive centers is mostly empirical. A considerable improvement of the benefits in the combination of homogeneous and heterogeneous catalysis was obtained by introduction of the concept of the interphase which is derived from reversed phase chromatography.^{3–5}

Interphases are systems in which a stationary phase and a mobile component penetrate each other on a molecular scale without forming a homogeneous phase. In ideal interphase regions reactive centers remain highly mobile and simulate the properties of a solution. Simple recovery of catalysts by filtration and a control of activity and selectivity is guaranteed, the leaching is largely reduced, and the reactivity can be modified by the employment of copolymers.⁶

The sol–gel process⁷ is a versatile method capable of generating inorganic–organic hybrid polymers with excellent swelling abilities and high accessibility for even large substrates. If transition metal complexes are provided with T-silyl functionalities [$R'-Si(OR)_3$], they can be subjected to a sol–gel process to yield stationary phases.⁸ They consist of an inert polysiloxane matrix, a flexible hydrocarbon spacer, and the reactive center. The mobile phase is a gaseous

liquid or dissolved reactant or simply a solvent. The matrix located transition metal complexes are securely incorporated into the hybrid polymer, and sufficient swelling abilities of the matrix enable the accessibility of the reactive centers.

A perusal of Table 1 shows the diversity of the reactive centers, the spacers, and the polysiloxane matrices which were prepared over the last years.^{8–16} The phosphine ligands range from bulky to less sterically hindered mono-, bis-, and trisphosphines linked via one, two, and three hydrocarbon chains of different lengths, respectively, to the polymer. The metal complexes cover the coordination geometries of cis and trans square planar and octahedral. Moreover the metal centers are connected to one, two, and three phosphines, respectively. The spacers not only differ in their lengths but also vary in their shape and polarity (alkane, PEG). The backbones of the polysiloxane matrices are built by simple cocondensing agents such as $Me_2(SiOMe)_2$ (D-type), $Me(SiOMe)_3$ (T-type), and $Si(OMe)_4$ (Q-type) (Figure 1)¹⁷ as well as by specially designed cocondensing agents [$H_3C(MeO)_2Si(CH_2)_zSi(OMe)_2CH_3$, $H_3C(MeO)_2Si(CH_2)_z(C_6H_4)-(CH_2)_zSi(OMe)_2CH_3$, (quasi Q-type)].^{10,18,19} The cocondensing agents are the components which modulate the stationary phase from rigid to highly mobile. They are also responsible for the porosity and swelling ability of the materials—these effects are a function of the degree of cross-linking within the polymer matrix. It is clear that the number of parameters and properties to describe these inorganic-organometallic hybrid catalysts increases with each new material designed. This complicates a comparison of these materials with common analytical and statistical methods.

Artificial Neural Networks (ANNs) have been successfully used in chemistry for pattern recognition and multivariate data analysis.²⁰ Since the beginning of the 1980s ANNs have become a rapidly growing field in computer science, and at present a wide range of different ANN algorithms and

* Corresponding authors: (E.L.) phone: +49-(0)7071-2972039; fax: +49-(0)7071-295306; e-mail: ekkehard.lindner@uni-tuebingen.de; (W.R.) phone: +49-(0)7071-2975482; fax: +49-(0)7071-295062; e-mail: rosenstiel@informatik.uni-tuebingen.de; (H.A.M.) phone: +49-(0)7071-2976229; e-mail: hermann.mayer@uni-tuebingen.de.

Table 1. Inorganic–Organic Hybrid Polymers Characterized by Solid State NMR Spectroscopy

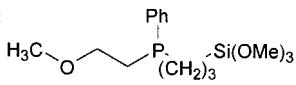
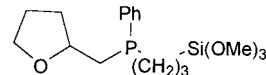
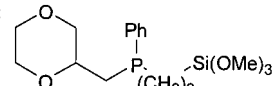
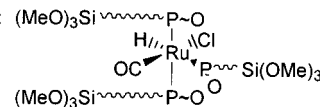
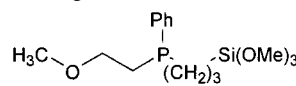
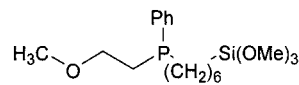
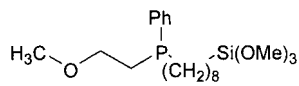
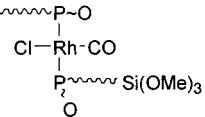
entry	chemical structure	ideal stoichiometry	ref
1	ligand A : 	T:Q = 1:2	8
2	cocondensed with Si(OCH ₃) ₄ ligand B : 	T:Q = 1:2	8
3	cocondensed with Si(OCH ₃) ₄ ligand C : 	T:Q = 1:2	8
4	cocondensed with Si(OCH ₃) ₄ complex I : 	with ligand A T:Q = 1:6	8
5	cocondensed with Si(OCH ₃) ₄ complex I with ligand B , cocondensed with Si(OCH ₃) ₄	T:Q = 1:6	8
6	complex I with ligand C , cocondensed with Si(OCH ₃) ₄	T:Q = 1:6	8
7	ligand A : 	T:D = 1:1.5	9
8	cocondensed with (H ₃ C) ₂ Si(OCH ₃) ₂ ligand D : 	T:D = 1:1.1	9
9	cocondensed with (H ₃ C) ₂ Si(OCH ₃) ₂ ligand E : 	T:D = 1:1.4	9
10	cocondensed with (H ₃ C) ₂ Si(OCH ₃) ₂ ligand A cocondensed with (H ₃ C)Si(OCH ₃) ₃	T:T = 1:2	9
11	ligand D cocondensed with (H ₃ C)Si(OCH ₃) ₃	T:T = 1:2	9
12	ligand E cocondensed with (H ₃ C)Si(OCH ₃) ₃	T:T = 1:2	9
13	ligand A cocondensed with Si(OCH ₃) ₄	T:Q = 1:2	9
14	ligand D cocondensed with Si(OCH ₃) ₄	T:Q = 1:2	9
15	ligand E cocondensed with Si(OCH ₃) ₄	T:Q = 1:2	9
16	complex I with ligand A cocondensed with (H ₃ C) ₂ Si(OCH ₃) ₂	T:D = 3:4.6	9
17	complex I with ligand D cocondensed with (H ₃ C) ₂ Si(OCH ₃) ₂	T:D = 3:3.3	9
18	complex I with ligand E cocondensed with (H ₃ C) ₂ Si(OCH ₃) ₂	T:D = 3:1.5	9
19	complex I with ligand A cocondensed with (H ₃ C)Si(OCH ₃) ₃	T:T = 1:2	9
20	complex I with ligand D cocondensed with (H ₃ C)Si(OCH ₃) ₃	T:T = 1:2	9
21	complex I with ligand E cocondensed with (H ₃ C)Si(OCH ₃) ₃	T:T = 1:2	9
22	complex I with ligand A cocondensed with Si(OCH ₃) ₄	T:Q = 1:2	9
23	complex I with ligand D cocondensed with Si(OCH ₃) ₄	T:Q = 1:2	9
24	complex I with ligand E cocondensed with Si(OCH ₃) ₄	T:Q = 1:2	9
25	ligand A cocondensed with cocondensing agent a : Me(MeO) ₂ Si—(CH ₂) ₆ —Si(OMe) ₂ Me	T:D = 1:1	10
26	ligand A cocondensed with cocondensing agent b : Me(MeO) ₂ Si—(CH ₂) ₈ —Si(OMe) ₂ Me	T:D = 1:1	10
27	ligand A cocondensed with cocondensing agent c : Me(MeO) ₂ Si—(CH ₂) ₁₄ —Si(OMe) ₂ Me	T:D = 1:1	10
28	complex II : 	with ligand A T:D = 2:1	10
29	cocondensed with cocondensing agent a complex II cocondensed with cocondensing agent a	T:D = 1:1	10
30	complex II cocondensed with cocondensing agent a	T:D = 1:2	10
31	complex II cocondensed with cocondensing agent a	T:D = 1:4	10
32	complex II cocondensed with cocondensing agent a	T:D = 1:8	10
33	complex II cocondensed with cocondensing agent a	T:D = 1:16	10
34	complex II cocondensed with cocondensing agent b	T:D = 1:1	10
35	complex II cocondensed with cocondensing agent c	T:D = 1:1	10

Table 1 (Continued)

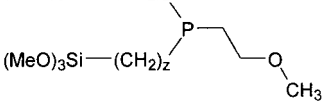
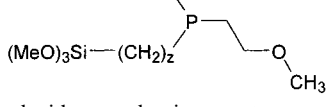
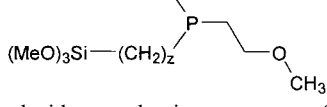
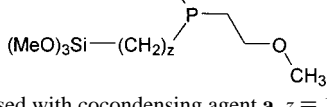
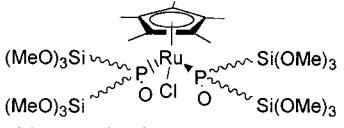
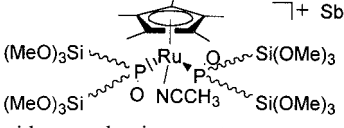
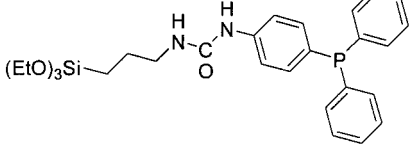
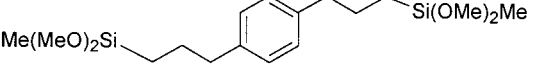
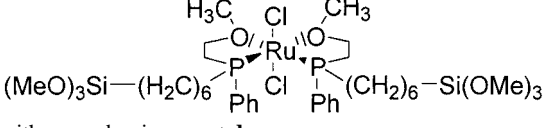
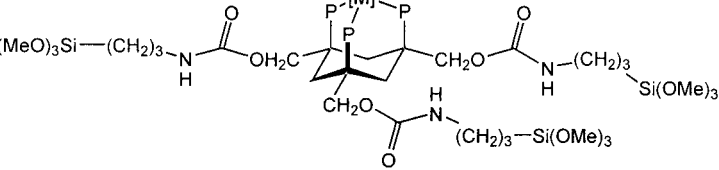
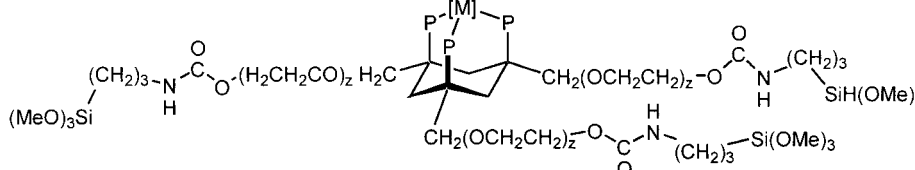
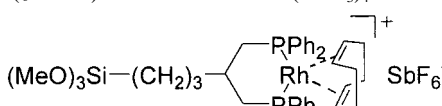
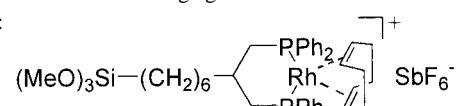
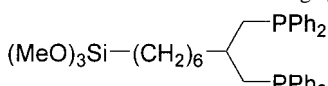
entry	chemical structure	ideal stoichiometry	ref
36	ligand F : $(\text{MeO})_3\text{Si}-(\text{CH}_2)_z$ 	T:D = 2:1	11
37	cocondensed with cocondensing agent a , $z = 3$ ligand G : $(\text{MeO})_3\text{Si}-(\text{CH}_2)_z$ 	T:D = 2:1	11
38	cocondensed with cocondensing agent a , $z = 6$ ligand G cocondensed with cocondensing agent a , $z = 6$	T:D = 1:1	11
39	ligand G cocondensed with cocondensing agent a , $z = 6$	T:D = 1:2	11
40	ligand H : $(\text{MeO})_3\text{Si}-(\text{CH}_2)_z$ 	T:D = 2:1	11
41	cocondensed with cocondensing agent a , $z = 8$ ligand K : $(\text{MeO})_3\text{Si}-(\text{CH}_2)_z$ 	T:D = 2:1	11
42	cocondensed with cocondensing agent a , $z = 14$ complex III :  with ligand F	T:D = 4:1	11
43	cocondensed with cocondensing agent a complex III with ligand G cocondensed with co condensing-agent a	T:D = 4:1	11
44	complex III with ligand H cocondensed with co condensing-agent a	T:D = 4:1	11
45	complex IV :  $\text{[}]^+ \text{SbF}_6^-$ with ligand G cocondensed with cocondensing agent a	T:D = 1:1	11
46	ligand L : 	T:D = 1:5	12
47	cocondensed with cocondensing agent a ligand L cocondensed with cocondensing agent d : 	T:D = 1:5	12
48	complex VI : 	T:D = 1:6	13
49	cocondensed with cocondensing agent d complex VII : 	T:Q = 1:0	14
50	cocondensed with itself, [M] = $\text{Mo}(\text{CO})_3$ complex VII cocondensed with $\text{Si}(\text{OCH}_3)_4$	T:Q = 1:1	14
51	complex VII cocondensed with $\text{Si}(\text{OCH}_3)_4$	T:Q = 1:4	14

Table 1 (Continued)

entry	chemical structure	ideal stoichiometry	ref
52	complex VIII : 	T:Q = 1:0	14
53	cocondensed with itself, [M] = Mo(CO) ₃ ; z = 9		
53	complex VIII (z = 9) cocondensed with Si(OCH ₃) ₄	T:Q = 1:1	14
54	complex VIII (z = 9) cocondensed with Si(OCH ₃) ₄	T:Q = 1:4	14
55	complex VIII (z = 120) cocondensed with itself	T:Q = 1:0	14
56	complex VIII (z = 120) cocondensed with Si(OCH ₃) ₄	T:Q = 1:1	14
57	complex VIII (z = 120) cocondensed with Si(OCH ₃) ₄	T:Q = 1:4	14
58	complex VIII (z = 230) cocondensed with itself	T:Q = 1:0	14
59	complex VIII (z = 230) cocondensed with Si(OCH ₃) ₄	T:Q = 1:1	14
60	complex VIII (z = 230) cocondensed with Si(OCH ₃) ₄	T:Q = 1:4	14
61	complex VIII (z = 270) cocondensed with itself	T:Q = 1:0	14
62	complex VIII (z = 270) cocondensed with Si(OCH ₃) ₄	T:Q = 1:1	14
63	complex VIII (z = 270) cocondensed with Si(OCH ₃) ₄	T:Q = 1:4	14
64	complex IX : 	T:D = 1:20	15
	cocondensed with cocondensing agent d		
65	complex X : 	T:D = 1:0	15
	cocondensed with itself		
66	complex X cocondensed with cocondensing agent a	T:D = 1:5	15
67	complex X cocondensed with cocondensing agent a	T:D = 1:20	15
68	complex X cocondensed with cocondensing agent d	T:D = 1:5	15
69	complex X cocondensed with cocondensing agent d	T:D = 1:20	15
70	ligand L : 	T:D = 1:5	16
	cocondensed with cocondensing agent d		
71	ligand L cocondensed with cocondensing agent d	T:D = 1:10	16
72	ligand L cocondensed with cocondensing agent a	T:D = 1:10	16

principles is available.²¹ All ANNs acquire knowledge about a certain problem from studying a set of data—called the training data set. Two fundamentally different learning strategies can be applied: supervised and unsupervised learning. In the first case, a set of corresponding correct answers (desired outputs) has to be presented for the training data set. Hence the learning procedure can employ this knowledge (that has to be possessed in advance). For unsupervised learning, no prior knowledge is utilized in the training process. All information has to be extracted from the data automatically.

In contrast to common statistical methods, ANNs are not restricted to linear correlations or linear subspaces. They can take into account nonlinear structures and structures of arbitrarily shaped clusters or curved manifolds. Therefore they can be applied effectively and efficiently for classification (identifying objects), prediction (modeling of functional correlation), and visualization (reducing dimensions).

In this study, Kohonen's Self-Organizing Feature Map (SOM)²² is employed as a tool to visualize structures in the NMR spectroscopic derived data set that characterize the stationary phases and to unfold hidden information. The

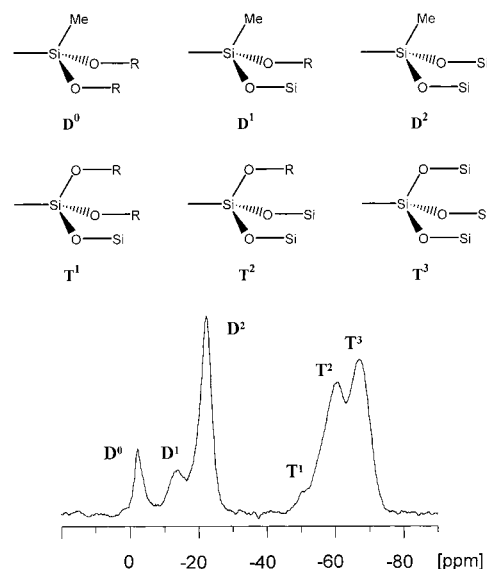


Figure 1. Sample (solid state) ²⁹Si CP/MAS NMR spectrum, featuring D- and T-type silicon groups with their subspecies D⁰-D² and T¹-T³.

Table 2. NMR Spectroscopic Derived Data of Compounds **1–72**

entry	T _{PH} [ms]	T _{1RH} (P) [ms]	T _{1RH} (Si) [ms]	T ⁰	T ¹	T ²	T ³	D	T	Q	type ^a
1	0.58	2.9	2.5			21.8	93.1		94	84	Q
2	0.23	4.4	3.7			25.9	66.7		91	82	Q
3	0.24	4.9	4			24.7	87.6		93	84	Q
4	0.22	5.8	5.5			32.3	68.8		86	83	Q
5	0.17	6.1	5.4			33	68.1		86	83	Q
6	0.18	6.2	5.4			32.3	61.5		83	81	Q
7	2.01	6.9	3.6			20.1	51.8	96	91		D
8	1.79	3.6	4.3			27	73	98	91		D
9	2.15	7.2	5.1				71.4	100	100		D
10	0.36	1.6	2.2		4	29.3	100		91		T
11	0.56	1.1	2.9			28.2	100		93		T
12	0.71	2	2.3			25	100		93		T
13	0.29	1.4	2.5			21.8	93.1		94	84	Q
14	0.32	1.4	1.6			25.7	69.5		91	86	Q
15	0.52	1.4	3.4			56.8	48.4		82	78	Q
16	0.22	3.8	6		2.4	37.4	41.4	88	83		D
17	0.2	4.3	5.1		7.5	56.7	85.1	82	84		D
18	0.23	4.5	5.1		16.7	100	91.7	80	78		D
19	0.2	2.8	5.2		19.6	58.9	100		82		T
20	0.21	5.6	5.4		3.2	58.1	100		87		T
21	0.2	4.1	5.2		7.4	77.8	100		83		T
22	0.23	2.6	5.5		6.5	32.3	68.8		86	83	Q
23	0.2	4.8	5.3		2.5	67.9	53.1		80	83	Q
24	0.2	4.9	5			39.7	36.6		83	80	Q
25	0.64	2	2.1			15.5	44.3	88	91		D
26	0.56	2.1	2.5			13.8	40.4	93	92		D
27	0.91	2.1	2			22.6	36.1	96	87		D
28	0.26	4.7	6.5		29.2	99	100	75	77		D
29	0.22	5.4	5.5		6.5	30.9	45.1	73	82		D
30	0.27	5.1	6.7			9.2	23.9	83	91		D
31	0.27	4.8	6.5			4.5	11.7	82	91		D
32	0.25	5.6	8.8			2.2	4.9	86	90		D
33	0.27	4	5.8			1.1	3.1	86	91		D
34	0.23	4.3	4.9		3.9	36.3	42.1	76	82		D
35	0.25	2.7	4.8		0.1	31.3	37.2	85	85		D
36	0.26	7.8	7.1			33.3	46.3	90.2	87.3		D
37	0.36	10	6.8			38.9	56.3	91.4	86.4		D
38	0.41	9.8	10.9			10.1	27.6	95.7	91		D
39	0.41	8.9	14.6			6.4	17.3	96.8	91.4		D
40	1.36	2	5.4			48.7	68	93	86.1		D
41	1.23	3.4	8.1			31.9	43.1	96	85.1		D
42	0.15	5.2	6.6		55.6	100	51	52.1	65.9		D
43	0.16	6.6	6.3		35.6	100	91	56.2	74.8		D
44	0.15	5.4	5.2		50.5	100	85.1	78	71.6		D
45	0.22	11.1	9.4			25.8	38.1	96	85.8		D
46	2.05	8.3	7.1			6.1	20.8	91.5	92.6		D
47	1.94	6.5	6.8			2.6	18.7	91.7	95.9		D
48	0.39	7.8	7.8			7.8	10.1	98.6	85.5		D
49	0.54	5.8	5.5	48	92.9	100	41.5		49.3		T
50	0.45	6.9	5.3	21	44.2	47.7	2.1		42.3	94.8	Q
51	0.63	6.5	4.9	7.1	15.6	15.7	2		43.5	88.6	Q
52	0.95	5.1	2.6	9.8	39.4	59.2	100		73		T
53	0.43	6.9	2.3	8.9	39.4	61.4	84.1		71.4	83.7	Q
54	0.69	6.6	2.2	2	10.2	13.1	15.1		67.4	85.9	Q
55	0.48	1.2	2.5		2.9	37.3	100		89.9		T
56	0.48	1.4	2		3.9	51.1	100		87.3	88.5	Q
57	0.55	1.5	1.8		1	14.2	28		87.4	90.1	Q
58	0.37	1.3	1.6				100		100		T
59	0.53	1.9	1.5			7.4	100		97.7	89.6	Q
60	0.49	2	1.5			3.2	37.2		100	93.1	Q
61	0.75	1.4	1.6				100		100		T
62	0.64	1.9	1.6				100		100	89.8	Q
63	0.74	1.7	1.5			2.6	30.7		97.4	91	Q
64	0.74	7.6	5.6			13.3	4.3	83.3	75.1		D
65	0.2	15	13.7			93.1	100		83.8		T
66	0.93	12	12.7			12.5	9.8	85.5	81.5		D
67	0.65	10.2	8			2.9	7.7	76.1	90.9		D
68	0.61	10.1	11.8			19.7	17.7	89.4	82.4		D
69	0.26	6.8	3.3				6.6	100	100		D
70	0.42	0.6	1.4			11.2	26.6	90	88		D
71	0.41	1.73	2.6			13.4	14.2	84	81		D
72	0.32	0.46	2.3			2.1	9.4	88	94		D

^a The “type” of the polymers refers to their composition regarding the cocondensing agents employed in their preparation, e.g. D:T polymer = D-type (see text and Table 1).

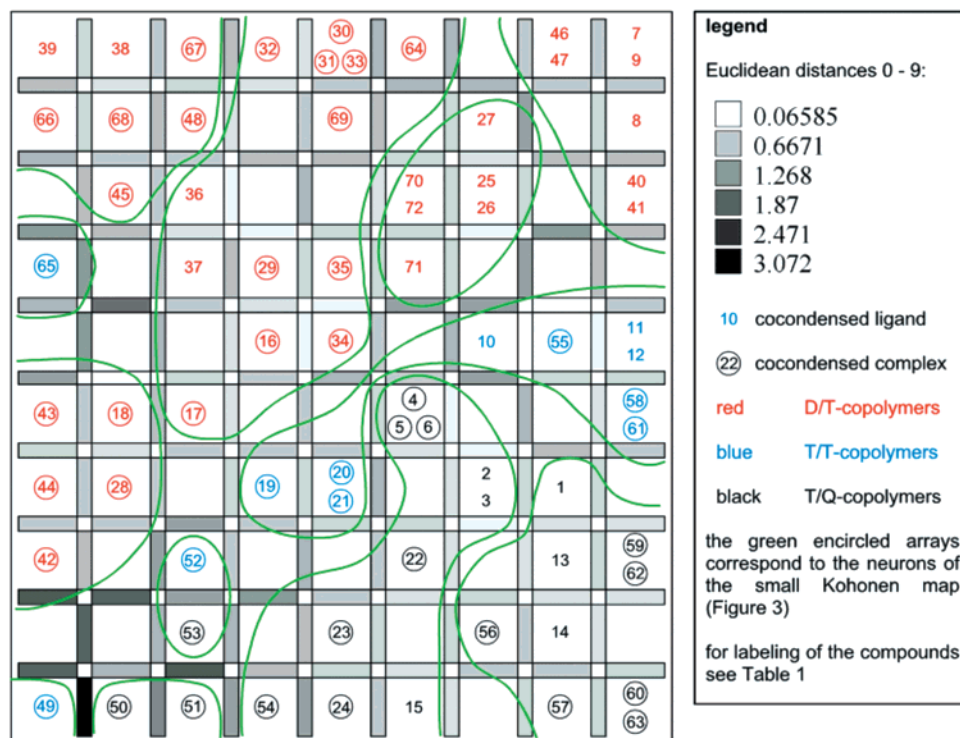


Figure 2. Combined (large) Kohonen and distance-map.

results of this visualization are used to compare inorganic–organic hybrid polymers that comprise different structural features and show different mechanical properties. Based on cross-linkage ($T^0 - T^3$, D, T, and Q) and NMR relaxation data (T_{PH} , $T_{1\rho H}$) (see Table 2) correlations of these materials are extracted, which were not obvious beforehand.

The accumulation of huge experimental data sets can cause the data to become very complex; therefore, new methods are needed that discover and illustrate effectively their inherent structures. Due to its unique properties, SOM seems very well suited for such a problem, and indeed the results demonstrate that it can be applied to analyze NMR data successfully.

EXPERIMENTAL SECTION

Computational Methods. To analyze and visualize the NMR data set, a program written in C was employed, implementing the well-known self-organizing feature map of Kohonen. The NMR data were saved as ASCII, and some standard data preprocessing techniques were applied—standardizing and scaling. There are two possible reasons for missing values in Table 2. Either the value has been too low to measure (e.g. intensity of T^0 , T^1 , etc. has been too low) or the corresponding functional groups (D, T, Q) have not been present in the examined compound. In the first case, small values were inserted, that had to be significantly lower than any measured value. In the second case the absence of a functional group has been indicated by the input of a zero value.

These data were used to train the self-organizing feature map. Despite the term “self-organizing”, some parameters have to be supplied to the program. The most important parameter is the size of the desired map. For classification purposes there are some rules of thumb on how big (or small)

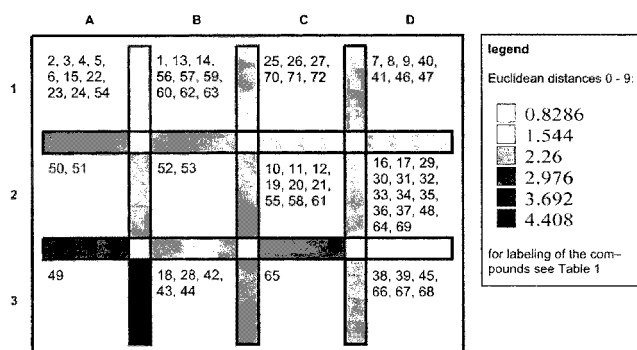


Figure 3. Combined (small) Kohonen and distance-map.

the map should be. If the map is used for visualization only, much larger maps have to be employed. Smaller maps can be applied to verify the results afterward. Other possible parameters include the adaptation function, adaptation height, and adaptation width at the beginning and at the end of the training and the number of training cycles. For each of these parameters standard parameters can be used. Best results are obtained, if the adaptation height and adaptation width are decreased exponentially during the training.²³ The resulting map is saved as ASCII and then visualized by other programs. To analyze the quality of the Kohonen-maps, component-maps, u-matrix-maps, and distance-maps were derived. Regarding these maps, statements are possible whether any folding or defects are present and how well the compounds are distributed or separated on the map. To better visualize the inherent structures of the Kohonen maps the big and the small map, each, have been combined with the corresponding distance-maps (Figures 2 and 3). These distance-maps are derived of the Euclidean distances between all the neurons on the Kohonen map.

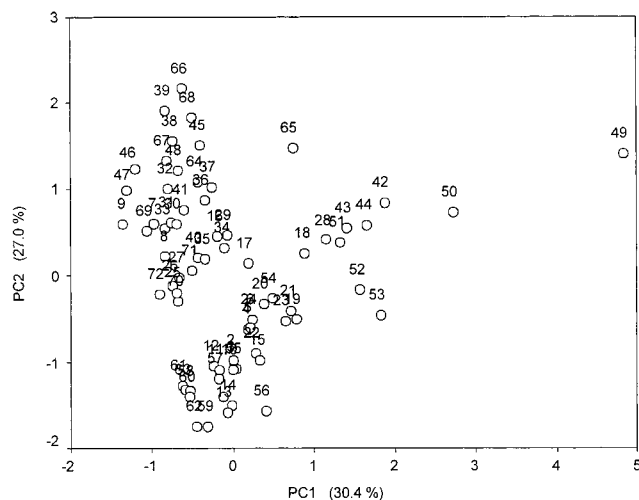


Figure 4. Principle component analysis of the NMR data set.

Each compound on this map is described by 10 parameters (Table 2). This can be regarded as a vector in a ten-dimensional data space where similar compounds are found close to each other. To visualize the neighborhoods and distribution in these data space, a mapping is required that projects the data on a two-dimensional plane while preserving the neighborhood relationships. The Kohonen Self-Organizing Feature Map provides such a nonlinear and topology-preserving mapping. Each position (neuron) on that two-dimensional map is associated with a weight vector (also called codebook-vector) and represents a region in the data space. Neurons that have the same distances on the map can have different distances in the data space. To visualize this fact, gray levels are introduced between each two neighboring neurons on the map. These gray levels correspond to the distances of the neurons in the data space. Usually these distances are measured by the Euclidean distances. Therefore, not only information about neighborhoods (similarities) in the data space but also about the distances are visualized.

To have a closer look on the distances the so-called u-matrix (Unified Matrix) provides a similar method.²⁴ If, for every neuron of the SOM, the distances to the eight immediate neighbors are summed up, a measure of dissimilarity between neurons in the ten-dimensional data space is obtained. This sum of distances for every neuron can be displayed by different gray levels and expressed as the u-matrix. Black neurons on the u-matrix represent large distances or borders between regions in the data space, while white neurons represent regions where neurons are located close to each other in the data space.

To justify the use of neural networks the results were compared with the most common data evaluation method—the principal component analysis (pca, Figure 4). These evaluations have been made using the commercially available product “SPSS” with the same preprocessed data as input.

NMR Data. The inorganic–organic hybrid polymers presented in Table 1 are prepared by hydrolytic sol–gel processes and are of completely amorphous nature. Thus solid-state NMR spectroscopy is an ideal tool to reveal structural and dynamic properties of these systems. The application of multinuclear CP/MAS NMR experiments allows the characterization of the structure of the polymer backbone, the local surroundings of the metal centers, and

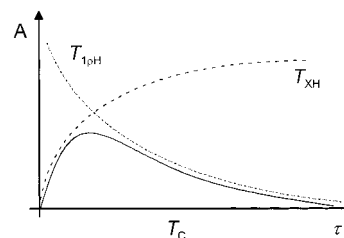


Figure 5. Schematic plot of signal intensity **A** versus time τ in a cross-polarization (CP) NMR experiment.

the functional groups of the ligands.^{25–27} By investigation of dynamic NMR parameters it is possible to quantify the solid-state NMR spectra.^{8,28} These results permit an insight into the degrees of hydrolysis and condensation, i.e., the cross-linkage of the polymer network and the quality of the sol–gel process applied. Dynamic NMR measurements also deliver a set of relaxation time data, which contribute to the data set to be evaluated by the neural network.

To monitor the mobility of the dry polymers measurements of the proton spin lattice relaxation time in the rotating frame $T_{1\rho H}$ are a common task (Table 2, columns 2 and 3).²⁹ This parameter covers a temporal range of a few milliseconds and corresponds to molecular motions in the kHz region. It is determined in a series of multinuclear (^{29}Si or ^{31}P) CP/MAS NMR experiments in which spin lock times, τ , are varied. The analysis of the series of intensities of a given signal in the multinuclear NMR spectra by fitting them to eq 1 provides the $T_{1\rho H}$ value for the investigated polymer.³⁰

$$I(\tau) = I(0)e^{-\tau/T_{1\rho H}} \quad (1)$$

If the sample polymer is built up homogeneously, strong dipole–dipole coupled protons throughout the whole system can be assumed and relaxation should be controlled by the spin-diffusion mechanism.^{31,32} In that case the determined $T_{1\rho H}$ value will be uniform for all protons throughout the sample.³³

Another parameter which reflects the mobility of the reactive center of a given compound is the cross-polarization constant T_{PH} for the phosphorus nucleus being under investigation (Table 2, column 1).²⁸ Figure 5 demonstrates schematically the evolution of a signal of a heteronucleus X in a cross-polarization NMR experiment in dependence on the contact time, T_C . The signal increase is determined by T_{XH} —which expresses equally the magnetization speed—while the signal decrease is determined by $T_{1\rho H}$. The cross-polarization constant T_{XH} is determined in the so-called “variable contact-time experiment”.³⁴ The quality and the speed of the magnetization transfer from the abundant proton spin system to the dilute heteronuclei spin system depends mainly on the amount of protons, their distance to the heteronuclei, and the mobility of the functional group containing the heteronucleus. An estimation of the mobility of two functional groups, therefore, is allowed only, if similar proton surroundings are present. With increasing mobility the magnetization transfer becomes slower, as a consequence of decreasing proton dipole–dipole interactions in the sample. Thus higher T_{XH} values indicate a higher mobility.^{35,36}

The parameters $T^0 - T^3$ represent the real signal intensities of the T subspecies in the ^{29}Si CP/MAS NMR spectra of the investigated polymers (Table 2, columns 4–7). They were calculated by eq 2 after determination of $T_{1\rho H}$, T_{SiH} ,

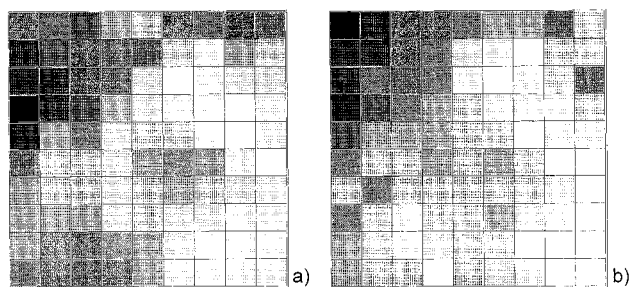


Figure 6. Component-maps of $T_{1\rho H}(P)$ (a) and $T_{1\rho H}(Si)$ (b). Higher values are represented by darker gray levels.

and the signal intensities in dependence of the contact time $I(T_C)$ by the above-mentioned dynamic NMR experiments.³⁴

$$I(T_C) = \frac{I_0}{(1 - T_{SiH}/T_{1\rho H})} (e^{-T_C/T_{1\rho H}} - e^{-T_C/T_{SiH}}) \quad (2)$$

In a subsequent step the degrees of condensation of the different silyl-functionalities D, T, and Q can be calculated (Table 2, columns 8–10).^{8,10} High degrees of condensation correspond to high cross-linking within the polymer matrix.

RESULTS AND DISCUSSION

The application of the Kohonen map proved to be a suitable method to visualize the experimental NMR data. Instead of numerous two-dimensional diagrams, one map including all information was obtained. A large number of inorganic–organic hybrid polymers (Table 1), that cannot be compared to each other directly, were evaluated and sorted.

The nonlinear topology-preserving Kohonen map showed clear advantages over traditional statistical methods such as principal component analysis (pca, Figure 4). If the scatter plot of the first two principal components is compared to the Kohonen map they look quite similar at first view. This is because pca also preserves distances. However, as it is limited to linear transformations, there are significant differences, and the first two principal components just cover 57.4% of the variance. Using this plot only two or three clusters can be delineated, and considering higher principal components the pca does not lead to a better separation of clusters. Furthermore, the pca becomes infeasible as the number of parameters increases. For n parameters $n(n-1)/2$ plots have to be examined. Considering the scatter plots and these limitations further interpretation of these plots is impracticable, and pca seems not to be suited for this kind of application.

Since a very large Kohonen map was chosen for visualization, the Euclidean distances between neighboring neurons are rather small; therefore, these distances or the derived u-matrix cannot be used to identify clusters automatically. Regarding the u-matrix-map (Figure 7b), no large white regions and no sharp borders are found. This indicates that a huge variety of compounds is distributed over big parts of our data space, expert know-how is required to interpret and validate the map. As soon as it is reduced to sizes that are usually used for classification, similar substances will be located on the same neuron, and a good separation with larger Euclidean distances is obtained—in this case clusters can be identified easily. Comparing the smaller map with the map which was applied for visualization, it is possible to verify

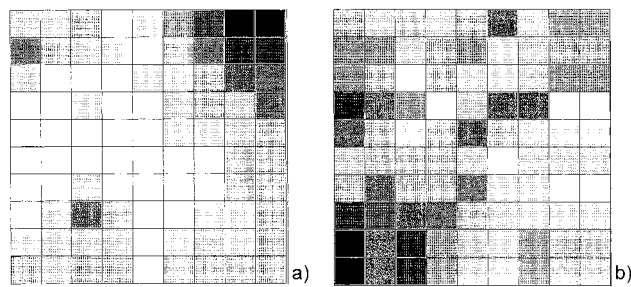


Figure 7. Component-map of T_{PH} (a) and u-matrix-map (b). Higher values are represented by darker gray levels.

whether any disadvantages or even errors have been acquired by employing such a large map. As it can be verified in Figures 2 and 3, the small map agrees with the larger map, as there is almost the same ordering (apart from being rotated or mirrored which does not have any effect on the neighborhood relationships or the distribution). Despite the fact that the maps were initialized randomly, and the data were sorted randomly at the beginning of the training, a great reproducibility is found. The only notable differences that were observed between several independent runs with the same data were mirrored or rotated maps, which do not affect the results.

The main criterion for the distribution of the compounds by the ANN is the presence or absence of values for the degree of condensation of the D-, T-, or Q-groups. Accordingly the output of the SOM is divided into three main sections, the D-, T-, and Q-domains (Figure 2, tagged red, blue and black, respectively). It is remarkable that the D- and Q-domains are separated by a strip of only T-cocondensed compounds. In fact, the “T-only” cocondensed polymers show physical and chemical properties which range between those of the D and the Q functionalized polymers, e.g. the degree of connectivity of the silyl groups, or the dynamic behavior.

The composition of the three different domains is determined by all ten NMR parameters, and it is not straightforward to decide which are the most significant. The component maps for the $T_{1\rho H}$ values measured by ^{29}Si or ^{31}P CP/MAS NMR spectroscopy, respectively, appear very similar (Figure 6). High $T_{1\rho H}$ values reside in the upper left part of the Kohonen map, while the lowest $T_{1\rho H}$ values are positioned in the lower right part. By way of contrast, the highest T_{PH} values are found in the upper right of the map (Figure 7a). Thus the main criteria for the arrangement within the D-domain are the relaxation times T_{PH} and $T_{1\rho H}$. A related sorting phenomenon is found in the T- and the Q-domains. The degree of condensation of the T-groups is a parameter that equally applies to all evaluated polymers. It influences mainly the position of the Q-type polymers on the map but in a more subordinate way than the values of the relaxation times do. Very low degrees of condensation of the T-groups are found in the lower left, while the highest degrees of condensation are found on the right side of the Kohonen map, with the main focus on the lower right side (Figure 8).

Most of the cocondensed ligands appear on the upper right half of the map (Figure 2), while the polymers containing cocondensed complexes mainly occupy the lower and the left half. To explain this fact the dynamic behavior of all compounds has to be taken into account. When the mobility of the polymers increases, the process of magnetization

39	38	67	32	30, 31 33	64		46	47	7	9
66	68	48		69		27			8	
	45	36			70, 72	25, 26			40, 41	
65		37	29	35	71					
			16	34		10	55		11, 12	
43	18	17			4, 5 6				58, 61	
44	28		19	20, 21		2, 3	1			
42		52			22		13		59, 62	
		53		23		56	14			
49	50	51	54	24	15		57		60, 63	

Figure 8. Component-map of the degrees of condensation of the T-groups. Light gray: degrees of condensation < 75%; dark gray: degrees of condensation > 95%.

transfer in a CP/MAS NMR experiment becomes slower and the T_{PH} values increase (vide supra). In general cocondensed ligands are more mobile than cocondensed complexes;^{9,10} therefore, ligands should be located in regions of the map in which the highest T_{PH} values are found (Figure 7a). In particular this is the case for the D-domain on the Kohonen map, but also in the T- and the Q-domains a concentration of ligands in specific areas is present.

The distribution of the polymers on the Kohonen map is influenced by their structural and dynamic properties which are partially a result of the sol–gel process applied. The way the sol–gel process proceeds depends on many different factors, like solvent employed, hydrolytic or non-hydrolytic route, concentration of the reaction partners, applied temperature, and others.^{7,37,38} The low range order within the polymers in the vicinity of the metal centers and the functional groups of the ligands is determined additionally by the molecular shape and the polarity of the educts. This may lead to template effects, especially in the surroundings of functional groups, which will be approximately the same if similar starting materials are employed for the sol–gel process. Therefore the steric, structural, and dynamic (NMR) parameters of polymers prepared in such a way must be roughly the same. The Kohonen map expresses this fact—without having knowledge about structural features of the polymers—by placing materials with similar structures in close vicinity on the map or even on the same neuron, as for example this is the case for compounds **1** and **13**, **4–6**, **7**, and **9**, or **59** and **62** (see more examples in Table 1 and Figure 2). The type of cocondensing agent and especially its stoichiometric amount in the polymer plays a major role regarding the physical properties of the polymers. This is the reason **18** and compounds **16** and **17** are separated on the small map although their chemical structures are almost identical. The same is true for compounds **50**, **51**, and **49**. In addition, **49** shows the lowest degree of condensation of the “T-only” cocondensed polymers which leads to a significant different pattern of signal intensities $T^0 - T^3$ in the ^{29}Si NMR spectra, compared to the adjacent polymers **50** and **51**. This fact explains the high Euclidean distances between these neighboring substances and the “isolation” of **49**. In contrast, the above explanation does not apply to compounds **1–3**. In these cases the structure of the cocon-

densed ligand is the decisive factor which separates them on the small map. The larger functional groups connected to the phosphine centers such as tetrahydrofuranyl and dioxanyl in **2** and **3** versus methoxyethyl in **1** lead to a smaller mobility of the former two polymers and higher $T_{1\rho H}$ values for **2** and **3** compared to **1**. The exposed position of compound **65** on the map is explained by the remarkable high values of $T_{1\rho H}$ and the low value of T_{PH} . Although this system is a “T-only” cocondensed polymer and the phosphine centers are anchored to the matrix by only one spacer it is one of the most rigid polymers presented in this work. The high Euclidean distances to the neighbors and its somewhat isolated position on the map reflect this fact.

The accumulation of similar structural characteristics of the compounds residing on neuron C2 of the small map (Figure 3) is noteworthy. In this T-domain cluster trisphosphine complexes are gathered (**19–21** and **55**, **58**, **61**), likewise the ligands **10–12** forming the complexes **19–21** are present. The combination of these characteristics (trisphosphine complexes and the same or similar ligands) leads to polymers with similar dynamic properties. An analogous case is found on neuron D1, but the overlap of characteristics is not as obvious as in the former case. The main feature of these polymers (**7–9**, **40**, **41**, **46**, and **47**) assembled in this cluster is the representation of monodentate phosphine ligands. These compounds show similar molecular dynamics, although they were prepared with three different cocondensing agents and although the phosphine centers in **40** and **41** are double spaced, which is in contrast to the single spaced phosphines **7–9**, **46**, and **47**.

It is remarkable to see that many polymers, which are found in close vicinity on both of the Kohonen maps and which share similar but not equal structural features, create similar NMR data sets (e.g. **58** and **61**, **59** and **62**, or **60** and **63**). These results give evidence that specific physical properties, like a high or a low mobility, are achieved by different ways of modification of the polymers. For example the introduction of long hydrocarbon spacers in the ligands or in the cocondensing agents and or the choice of D-type cocondensing agents leads to highly mobile polymers.^{10,11} On the other hand, if rigid systems are favored the way of spacing (2- or 3-fold) or the application of other types of cocondensing agents (T-type or Q-type) are possible methods of polymer modification (examples for rigid systems are the polymers **4–6**, **22–24**, or **42–45**, examples for highly mobile systems are the polymers **7–9**, **25–27**, **40**, **41**, **46**, **47**).

CONCLUSION

Different inorganic–organic hybrid polymers with a variety of structural features have been evaluated successfully by the Kohonen’s Self-Organizing Feature Map. The output of the Kohonen map reveals information about similarities of the polymers that cannot be obtained by a principal component analysis. In particular with the help of the small Kohonen map it was demonstrated that certain polymers share the same dynamics, although their structural principles are quite different. This leads to the conclusion that the same dynamic effects (mobility – rigidity) can be evoked by different chemical and structural features (kind of spacer in the ligand or in the cocondensing agent or the type of cocondensing agent). Furthermore, since physical and me-

chanical properties of sol–gel prepared polymers also depend on the way the sol–gel process is carried out (choice of solvent, temperature, concentration, catalyst, etc.), it is obvious that sol–gel processing has to be standardized as well as uniform aging of the xerogels is important. Hence, since all these conditions are kept, the output of the Kohonen map, i.e., the visualization of the neighborhood relationships in the NMR data set, permits a correlation of structure and dynamics of these materials (Table 1 and Figure 2). To correlate the structural and dynamical features of these systems with their chemical behavior, information about catalytic activities and selectivities are of great value. Future evaluations of organometallic hybrid polymers by SOMs will consider these chemical aspects.

ACKNOWLEDGMENT

The support of this research by the Deutsche Forschungsgemeinschaft (Forscherguppe, Grant FOR 184/3-1 and Graduiertenkolleg, Grant GK – GRK 441/1-00), Bonn/Bad Godesberg, and by the Fonds der Chemischen Industrie, Frankfurt/Main, is gratefully acknowledged.

REFERENCES AND NOTES

- (1) Supported Organometallic Complexes. Part 28. Part 27: Lindner, E.; Brugger, S.; Steinbrecher, S.; Plies, E.; Seiler, M.; Bertagnolli, H.; Wegner, P.; Mayer, H. A. Novel sol–gel processed rhodium(I) complexes: synthesis characterization and catalytic reactions in interphases. *Inorg. Chim. Acta* **2002**, 327, 54–65.
- (2) Pomogailo, A. D. Specific Characteristics of Catalysis by Polymer-immobilised Complexes. *Russ. Chem. Rev.* **1992**, 61, 133–153.
- (3) Marqusee, J. A.; Dill, J. Solute Partitioning Into Chain Molecule Interphases. Monolayers, Bilayer Membranes, and Micelles. *J. Chem. Phys.* **1986**, 85, 434–444.
- (4) Sander, L. C.; Wise, S. A. In *Retention and Selectivity Studies in HPLC*; Smith, R. M., Ed.; Elsevier: Amsterdam, 1994; pp 337–369.
- (5) Dorsey, J. G.; Dill, K. A. The Molecular Mechanism of Retention in Reversed-phase Liquid Chromatography. *Chem. Rev.* **1989**, 89, 331–346.
- (6) Lindner, E.; Schneller, T.; Auer, F.; Mayer, H. A. Chemistry in Interphases-A New Approach to Organometallic Syntheses and Catalysis. *Angew. Chem.* **1999**, 111, 2288–2309; *Angew. Chem., Int. Ed. Engl.* **1999**, 38, 2154–2174.
- (7) Brinker, C. J.; Scherer, G. W. *Sol–Gel Science*; Academic Press: London, 1990.
- (8) Lindner, E.; Kemmler, M.; Mayer, H. A.; Wegner, P. Polysiloxane-Bound Ether-Phosphines and Ruthenium Complexes. A Characterization by Solid-State NMR Spectroscopy and Catalysis. *J. Am. Chem. Soc.* **1994**, 116, 348–361.
- (9) Lindner, E.; Jäger, A.; Schneller, T.; Mayer, H. A. Mobility Studies on Sol–Gel Processed Ether-Phosphines and Their Ruthenium(II) Complexes with Different Spacer Lengths. A Solid State NMR Study. *Chem. Mater.* **1997**, 9, 81–90.
- (10) Lindner, E.; Schneller, T.; Mayer, H. A.; Bertagnolli, H.; Ertel, T. S.; Hörner, W. Hydrocarbon-Bridged Methylmethoxysilanes as new Co-condensation Agents for the Sol–Gel Process of the Rhodium(I) Complex $\text{ClRh}(\text{CO})(\text{P}\sim\text{O})_2$ Containing the Ligand $\text{PhP}(\text{CH}_2\text{CH}_2\text{OCH}_3)(\text{CH}_2)_3\text{Si}(\text{OCH}_3)_3$. *Chem. Mater.* **1997**, 9, 1524–1537.
- (11) Lindner, E.; Wielandt, W.; Baumann, A.; Mayer, H. A.; Reinöhl, U.; Weber, A.; Ertel, T. S.; Bertagnolli, H. Sol–Gel Processed Phosphine Ligands with two T- or D-Silyl Functionalities and their $(\eta^5\text{-C}_5\text{Me}_5)\text{-Ru(II)}$ Complexes. *Chem. Mater.* **1999**, 11, 1833–1845.
- (12) Lindner, E.; Salesch, T. A general synthetic route for the synthesis of mono-T-silyl functionalized aromatic phosphines as ligands for chemistry in interphases. *J. Organomet. Chem.* **2001**, 628, 151–154.
- (13) Salesch, T. Synthesis and Characterization of Novel Functionalized Polysiloxanes and Their Application in Model and Catalytic Reactions and F_2' in Chromatography. Ph.D. Thesis, Universität Tübingen, 2001.
- (14) (a) Büchele, J. Ph.D. Thesis: Multikern-Festkörper-NMR-Spektroskopie zur Charakterisierung von Struktur und Dynamik stationärer Phasen sowie zur Hydratation zementgebundener Materialien; Universität Tübingen, 1999. (b) Büchele, J.; Mayer, H. A. Chemistry in Interphases. The solid-phase Synthesis of Well-Defined Rhodium and Iridium Phosphine Complexes. *Chem. Commun.* **1999**, 2165–2166.
- (15) Lindner, E.; Brugger, S.; Steinbrecher, S.; Plies, E.; Sailer, M.; Bertagnolli, H.; Wegner, P. Novel sol–gel processed rhodium(I) complexes: synthesis characterization and catalytic reactions in interphases. *Inorg. Chim. Acta* **2002**, 327, 54–65.
- (16) Lindner, E.; Brugger, S.; Steinbrecher, S.; Plies, E.; Mayer, H. A. Accessibility and solid-state NMR studies on sol–gel processed diphosphine ligands. *Z. Anorg. Allg. Chem.* **2001**, 627, 1731–1740.
- (17) Lippmaa, E.; Mägi, M.; Samson, A.; Engelhardt, G.; Grimmer, A.-R. Structural Studies of Silicates by Solid-State High Resolution ^{29}Si NMR. *J. Am. Chem. Soc.* **1980**, 102, 4889–4893. Q: quadrifunctional silicon; T: trifunctional silicon; D: difunctional silicon.
- (18) In this case “quasi Q-type” means four possible Si–O–Si bonds per molecule as in $\text{Si}(\text{OR})_4$.
- (19) Lindner, E.; Salesch, T.; Hoehn, F.; Mayer, H. A. Novel D- and T-functionalized Polysiloxane Matrices for Reactions in Interphases. *Z. Anorg. Allg. Chem.* **1999**, 625, 2133–2143.
- (20) Zupan, J.; Gasteiger, J. *Neural Networks for Chemists*; VCH Verlagsgesellschaft: Weinheim, 1993.
- (21) Zell, A. *Simulation Neuronaler Netze*; Addison-Wesley: Reading, MA, 1994.
- (22) Kohonen, T. Self-organized Formation of Topology Correct Feature Maps. *Biol. Cybern.* **1982**, 43, 59–69.
- (23) Göppert, J. *Die topologisch interpolierende selbstorganisierende Karte in der Funktionsapproximation*; Shaker Verlag: Aachen, 1996.
- (24) Ultsch, A. In *Information and Classification*; Opitz, O., Lausen, B., Klar, R., Eds.; Springer-Verlag: New York, 1993; pp 307–313.
- (25) Fyfe, C. A. *Solid State NMR for Chemists*; CRC Press: Guelph, ON, 1984.
- (26) Fyfe, C. A.; Zhang, Y.; Aroca, P. An Alternative Preparation of Organofunctionalized Silica Gels and Their Characterization by Two-dimensional High-resolution Solid-state Heteronuclear NMR Correlation Spectroscopy. *J. Am. Chem. Soc.* **1992**, 114, 3252–3255.
- (27) Eckert, H. Structural Characterization of Noncrystalline Solids and Glasses Using Solid State NMR. *Prog. Nucl. Magn. Reson. Spectrosc.* **1992**, 24, 159–293.
- (28) Voelkel, R. High-resolution Solid-state ^{13}C NMR Spectroscopy of Polymers. *Angew. Chem.* **1988**, 100, 1525–1540; *Angew. Chem., Int. Ed. Engl.* **1988**, 27, 1468.
- (29) Aujla, R. S.; Harris, R. K.; Packer, K. J.; Parameswaran, M.; Say, B. J.; Bunn, A.; Cudby, M. E. A. Discriminatory Experiments in High-Resolution ^{13}C NMR of Solid Polymers. *Polym. Bull.* **1982**, 8, 253–259.
- (30) Koenig, J. L.; Andreis, M. In *Solid State NMR of Polymers*; Mathias, L. J., Ed.; Plenum Press: New York, 1991; pp 201–213.
- (31) Abragam, A. *The principles of Nuclear Magnetism*; Clarendon Press: Oxford, 1961; pp 138, 139.
- (32) Spiess, H. W. Structure and Dynamics of Solid Polymers from 2D- and 3D-NMR. *Chem. Rev.* **1991**, 91, 1321–1328.
- (33) McBrierty, V. J.; Douglass, D. C. Recent Advances in the NMR of Solid Polymers. *J. Polym. Sci., Part D: Macromol. Rev.* **1981**, 16, 295–366.
- (34) Mehring, M. *Principles of High-Resolution NMR in Solids*; Springer-Verlag: New York, 1983.
- (35) McArthur, D. A.; Hahn, E. L.; Walstadt, R. E. Rotating-frame Nuclear-double-resonance Dynamics: Dipolar Fluctuation Spectrum in Calcium Fluoride. *Phys. Rev.* **1969**, 188, 609.
- (36) Schaefer, J.; Stejskal, E. O.; Buchdal, R. Magic-angle ^{13}C NMR Analysis of Motion in Solid Glassy Polymers. *Macromolecules* **1977**, 10, 384–405.
- (37) Hench, L. L.; West, J. K. The Sol–gel Process. *Chem. Rev.* **1990**, 90, 33–72.
- (38) Cerveau, G.; Corriu, J. P.; Framery, E. Sol–gel process: Influence of the Temperature on the Textural Properties of Organosilsequioxane Materials. *J. Mater. Chem.* **2000**, 10, 1617–1622.

CI010373Z